Asymptotically inspired moment-closure approximation for adaptive networks

Maxim S. Shkarayev[1] and Leah B. Shaw[2]
[1]*Department of Physics and Astronomy, Iowa State University, Ames, Iowa 50011, USA*
[2]*Department of Applied Science, College of William & Mary, Williamsburg, Virginia 23187, USA*
(Received 6 March 2013; published 6 November 2013)

Adaptive social networks, in which nodes and network structure coevolve, are often described using a mean-field system of equations for the density of node and link types. These equations constitute an open system due to dependence on higher-order topological structures. We propose a new approach to moment closure based on the analytical description of the system in an asymptotic regime. We apply the proposed approach to two examples of adaptive networks: recruitment to a cause model and adaptive epidemic model. We show a good agreement between the improved mean-field prediction and simulations of the full network system.

DOI: 10.1103/PhysRevE.88.052804 PACS number(s): 89.75.Hc, 87.10.Mn, 05.10.Gg

I. INTRODUCTION

In recent years we have seen much progress in the field of network dynamics and dynamics on networks [1–4]. Strong interest in understanding phenomena such as disease spread in social networks, interaction online social media such as Facebook and Twitter, dynamics of neuronal networks, and many others have encouraged development of mathematical tools necessary to analyze the behavior of such systems [5–9].

Often the first step in analyzing such systems is to represent them as networks, where an individual unit, e.g., a person, a user account, or a neuron, is represented by a node, and the possibility of interaction between any two units is represented by a link between them. The dynamical processes on such networks are often characterized by their statistical properties via a mean-field approach [10–13]. Such mean-field equations consist of a hierarchy of equations, where the expected state of the nodes, due to interaction via the network, is coupled to the statistical description of links in the network. The dynamical evolution of the links in turn depends on the evolution of statistical description of node triples, which in turn depend on higher-order structures, and so on. In other words, this mean-field description yields an infinite system of coupled equations, which usually must be truncated in order to be solvable. The truncated system is open and has to be closed by introducing additional information about the system.

The dynamics on network systems are often closed at the level of link equations, where the network information makes its first appearance [14]. Perhaps the simplest closure approach is based on the assumption of homogeneous distribution of different node types in the system and that the probability of finding a particular type of node in the neighborhood of a given node is independent of what else can be found in that node's neighborhood. This closure was shown to produce excellent results for many different systems [14–19]. On the other hand, the heterogeneous mean-field approach, where conditioning on the total degree of nodes is introduced, may improve the accuracy of the approximation, although drastically increasing the number of equations in the description [9,20]. Often, additional information about the system, such as the expected clustering coefficient, may be used to improve the closure [17]. In other cases, assumptions about the shape of degree distribution functions [19], possibly guided by numerical simulations or physical observations [15,21], may lead to an improvement in closure. Equation-free approaches may also be used when closing the mean-field equations [22,23].

All of the above closures often lead to a reasonable approximation of the system dynamics. However, they all suffer either from the lack of *a priori* knowledge of the validity of approximation or from having an excessive number of equations that must be analyzed. In this paper, we propose a new method that may lead to accurate closures and that also allows one to manage the expectation of the accuracy of the obtained closure. The proposed approach is based on simplification of the mean-field system of equations in some asymptotic regime. In the rest of the paper we demonstrate our approach by applying it to two adaptive network systems, i.e., networks where dynamical processes on the nodes affect the network structure, which in turn affects subsequent dynamics on the nodes [24]. In Sec. II we derive an improved closure for an adaptive epidemic model [10]. In Sec. III, we derive a closure for a system modeling recruitment to a cause [12].

II. ADAPTIVE EPIDEMIC MODEL

Our first example is a model for epidemic spread in an adaptive social network [10]. Here the disease spread is described using the susceptible-infected-susceptible model, where each individual in the society is in one of the two states: sick or *infected* and healthy but *susceptible* to infection. In the framework of networks, we refer to these as I and S nodes, respectively. The infected individuals become susceptible at recovery rate r. The disease can spread at a rate p from infected individuals to susceptible ones via a contact between them, where the existence of the contact is defined by the network structure. The adaptation mechanism allows susceptible individuals to change their local connectivity to avoid contact with infected individuals. Thus, the susceptibles rewire their contacts away from infecteds at rate w, connecting instead to a randomly chosen susceptible. The node and link dynamical rules are summarized in the Figs. 1(a) and 1(b), respectively.

In order to describe the evolution of this system, we begin with developing a heterogeneous mean-field description [20]. We characterize the time evolution of $\rho_{\alpha;\mathbf{k}}$, the expected number of nodes of type α with k_1 and k_2 nodes of type S and I, respectively, in their neighborhoods,

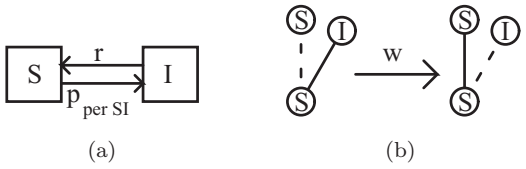

FIG. 1. Schematic representation of (a) node dynamical rules and (b) link dynamical rules in the adaptive epidemic model.

where $\mathbf{k} = (k_1, k_2)$,

$$\partial_t \rho_{S;\mathbf{k}} = r\rho_{I;\mathbf{k}} - pk_2\rho_{S;\mathbf{k}} + \sum_i [\Omega_{S;\mathbf{k}-r_i}(r_i)\rho_{S;\mathbf{k}-r_i} - \Omega_{S;\mathbf{k}}(r_i)\rho_{S;\mathbf{k}}], \quad (1a)$$

$$\partial_t \rho_{I;\mathbf{k}} = -r\rho_{I;\mathbf{k}} + pk_2\rho_{S;\mathbf{k}} + \sum_i \left[\Omega_{I;\mathbf{k}-r_i}(r_i)\rho_{I;\mathbf{k}-r_i} - \Omega_{I;\mathbf{k}}(r_i)\rho_{I;\mathbf{k}}\right]. \quad (1b)$$

The allowed the transitions and corresponding rates shown in Table I. In the transition rates table, the function K (function M) corresponds to the expected number of node chains that originate at an S node (I node) with a neighborhood specified by $\mathbf{k}$, which connects to an S node, which in turn connects to an I node. The terms $N_{X_1 \ldots X_n}$ correspond to the expected number of node chains in the system, where a node chain constitutes a set of nodes, connected as follows: a node of type X_1 is connected to the node of type X_2, which in turn is connected to node of type X_3, and so on. For example, N_S is the expected number of S nodes in the network, while N_{IS} is the expected number of links with S and I nodes at its ends. In our definition of node chains we require the ith and $i+1$st nodes to differ; however, ith and $i+2$nd nodes can in fact be the same node. In the example of a network presented in Fig. 2(a) there are four ISI triples, corresponding to the following node combinations: 1-2-1, 1-2-3, 3-2-1, and 3-2-3. It should be noted that whether or not nodes 1 and 3 are connected is irrelevant to this definition. Also note that the order in which the nodes appear matters, which, for example, means that N_{SS} corresponds to twice the expected number of undirected links between two susceptible nodes.

The heterogeneous mean-field equations are high dimensional and, therefore, are extremely difficult to analyze. A common way to analyze the dynamics of social networks is via lower-dimensional mean-field equations. These are typically obtained by simply writing down rates of change for nodes and links, based on an intuitive understanding of the dynamics, such as in Refs. [10,11]. Here, however, we will derive them formally from the heterogeneous mean-field system so the procedure and assumptions are clear. The lower-dimensional mean-field equations are generated by

TABLE I. Transitions and nonzero transition rates in Eq. (1).

Transitions	Nonzero rates
$r_1 = (1,-1)$	$\Omega_{I;\mathbf{k}}(r_1) = \Omega_{S;\mathbf{k}}(r_1) = rk_2$
$r_2 = (-1,1)$	$\Omega_{S;\mathbf{k}}(r_2) = pK(\mathbf{k})$, $\Omega_{I;\mathbf{k}}(r_2) = pM(\mathbf{k})$
$r_3 = (1,-1)$	$\Omega_{S;\mathbf{k}}(r_3) = wk_2$
$r_4 = (1,0)$	$\Omega_{S;\mathbf{k}}(r_4) = wN_{\mathrm{IS}}/N_S$
$r_5 = (-1,0)$	$\Omega_{I;\mathbf{k}}(r_5) = wk_1$

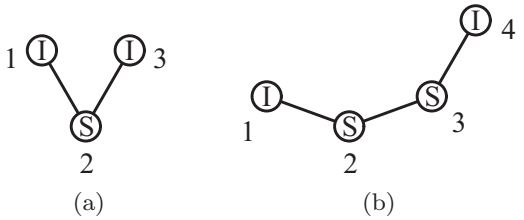

FIG. 2. (a) Schematic representation of an I-S-I triple. (b) Schematic representation of four-node chains I-S-S-I. The term N_{ISSI} corresponds to the expected number of such chains.

multiplying the heterogeneous mean-field equations by $k_1^{i_1}k_2^{i_2}$ for some non-negative integer values of i_j and summing over $\mathbf{k}$. Thus, the equations describing node dynamics are obtained by taking $i_1 + i_2 = 0$, as given in Eqs. (A1a) and (A1b) of Appendix A, while the description of the link dynamics is obtained by taking $i_1 + i_2 = 1$, as given in Eqs. (A1c)–(A1e).

The hierarchy of equations generated in this manner must be truncated in order to obtain a finite-dimensional description of the system. Such truncation leaves the system open and in need of closure. For example, the system of node and link equations in (A1) contains the terms N_{SSI} and N_{ISI}, which describe higher-order structures. The usual approach to closure [15] comes from the assumption of homogeneous distribution of the I nodes in the neighborhood of S nodes, which leads to the following closure equations:

$$\frac{N_{\mathrm{SSI}}}{N_S} = \frac{N_{\mathrm{SS}}}{N_S}\frac{N_{\mathrm{IS}}}{N_S}, \quad (2a)$$

$$\frac{N_{\mathrm{ISI}}}{N_S} = \left(\frac{N_{\mathrm{IS}}}{N_S}\right)^2 + \frac{N_{\mathrm{IS}}}{N_S}, \quad (2b)$$

where we also assumed that the degree distribution of susceptible nodes is Poisson. The details of these closures are presented in the Appendix B.

These closures are based on *ad hoc* assumption and may fail to capture the system behavior accurately if, for example, correlations are present. Here we develop an approach that derives the closure based on the system behavior in some asymptotic regime.

We begin by generating equations for the time evolution of second moments by multiplying the heterogeneous mean-field equations by $k_1^{i_1}k_2^{i_2}$, with $i_1 + i_2 = 2$, and summing over $\mathbf{k}$. We consider a steady state of these equations, taken at some asymptotic limit. While we cannot provide an exact algorithm for deciding which limit to take, we rely on the fact that the number of parameters is finite and therefore all the possible limits can be considered. The choice of the particular limit is based on the condition that in this limit the higher-order moments, which are present in the second moment equations, approach zero or can be well approximated by the lower-order terms. Note that the resulting relation is accurate in the considered limit, i.e., it is not *ad hoc* and can be expected to perform well at least in the considered limit. In other words, this approach serves to decouple the first few moment equations from the rest of the equation hierarchy. We will derive a closure expression for the N_{ISI} term and numerically explore the performance of the derived closures, in parameter

regimes outside of the asymptotic limit and outside of the steady state.

A. Closure of ISI term

We derive a new closure of the ISI term by first considering the evolution of the number of ISI triples. Multiplying equation (1a) by k_2^2 and summing over $\mathbf{k}$ at steady state,

$$\sum_{\mathbf{k}} k_2^2 \partial_t \rho_{S;\mathbf{k}} = 0, \tag{3}$$

we obtain the following equation:

$$0 = rN_{\mathrm{III}} - p\sum_{\mathbf{k}}\left[k_2^3\rho_{S;\mathbf{k}}\right] + (r+w)[-2N_{\mathrm{ISI}} + N_{\mathrm{IS}}] + p[2N_{\mathrm{ISSI}} + N_{\mathrm{SSI}}], \tag{4}$$

where the four-point term ISSI corresponds to the total number of node configurations shown in Fig. 2(b). Details of the derivation of Eq. (4) are given in Appendix C. Using the steady-state relations in Eqs. (A3a) and (A3b), we arrive at

$$2(r+w)N_S\left(\frac{N_{\mathrm{ISI}}}{N_S} - \frac{N_{\mathrm{IS}}}{N_S} - \frac{N_{\mathrm{IS}}}{N_S}\frac{N_{\mathrm{ISSI}}}{N_{\mathrm{SSI}}}\right) = rN_I\left(\frac{N_{\mathrm{III}}}{N_I} - \frac{N_{\mathrm{II}}}{N_I}\frac{\sum_{\mathbf{k}}\left[k_2^3\rho_{S;\mathbf{k}}\right]}{\sum_{\mathbf{k}}\left[k_2^2\rho_{S;\mathbf{k}}\right]}\right). \tag{5}$$

The left-hand side of the equation corresponds to the flux of the expected number of ISI triples due to the changes in the neighborhood of the susceptible nodes, while the right-hand side corresponds to the flux due to the infection and recovery of the susceptible node in the ISI triple. In the limit of large infection rate and weak rewiring, the amount of time any node spends in the susceptible state approaches zero. Therefore, it is reasonable to assume that the flux of triples due to the changes in the neighborhood of the susceptible node will approach zero as well. This leads us to conclude that the two sides of Eq. (5) must vanish, leaving us with the following relation:

$$\frac{N_{\mathrm{ISI}}}{N_S} = \frac{N_{\mathrm{IS}}}{N_S} + \frac{N_{\mathrm{IS}}}{N_S}\frac{N_{\mathrm{ISSI}}}{N_{\mathrm{SSI}}}. \tag{6}$$

Finally, we note that the term $N_{\mathrm{ISSI}}/N_{\mathrm{SSI}}$ corresponds to the expected number of I nodes, node 1 in Fig. 2(b), attached to the chain of nodes numbered 2, 3, and 4 in that figure. This relation is well approximated by the homogeneity assumption that the information about the neighborhood of the third node in Fig. 2(b) has no effect on the information about the neighborhood of the second node. In other words, the following moment closure is considered:

$$\frac{N_{\mathrm{ISSI}}}{N_{\mathrm{SSI}}} = \frac{N_{\mathrm{SSI}}}{N_{\mathrm{SS}}}. \tag{7}$$

That is, we make a homogeneity assumption about the neighborhood of a neighbor, and we expect this assumption to be more accurate than the same assumption about a given node's neighborhood, i.e., the closures in Eqs. (2a) and (2b).

Thus, we have derived a new closure of N_{ISI},

$$\frac{N_{\mathrm{ISI}}}{N_S} = \frac{N_{\mathrm{IS}}}{N_S} + \frac{N_{\mathrm{IS}}}{N_S}\frac{N_{\mathrm{SSI}}}{N_{\mathrm{SS}}}, \tag{8}$$

which relies on our ability to close the N_{SSI} term, and this brings us one step closer to finding an accurate closure of the mean-field description of the adaptive epidemic model (A1). The closure of Eq. (8) is tested in Figs. 3 and 4, as is the homogeneity closure of Eq. (2b). We also show the relative

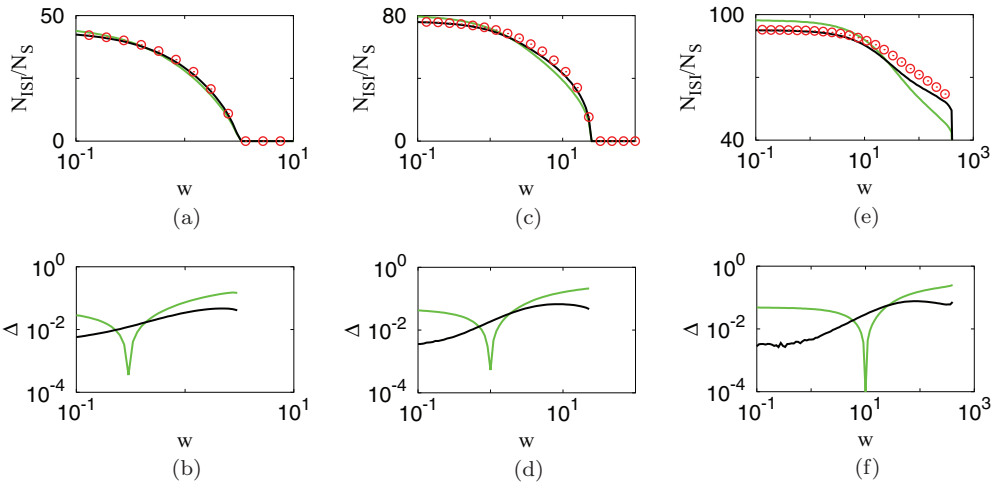

FIG. 3. (Color online) Number of ISI triples per S node as a function of rewiring rate w, for several infection rates p: simulations compared to the moment closure of Eq. (2b) and the newly derived closure of Eq. (8). The values of the infection rates are as follows: $p = 10^{-1/2}$ in (a) and (b), $p = 10^0$ in (c) and (d), and $p = 10^1$ in (e) and (f). Panels (a), (c), and (e) show N_{ISI}/N_S measured in simulation (circles, red online), approximated using the homogeneity closure of Eq. (2b) (light gray curve, green online), and approximated using the result of asymptotic analysis in Eq. (8) (dark gray curve, black online). The closures are evaluated using node and link quantities measured in the simulations. The light gray curves (green online) in panels (b), (d), and (f) show the relative error, Eq. (9), of the homogeneity approximation, Eq. (2b), while dark gray curves (black online) show the relative error due to the newly derived approximation, Eq. (8). Cusps in the relative error curves correspond to the N_{ISI}/N_S homogeneity closure curve crossing through the curve measured in simulations. Simulations are performed on a network with 10^5 nodes and 5×10^5 links, with $r = 1$, following algorithm in Ref. [25].

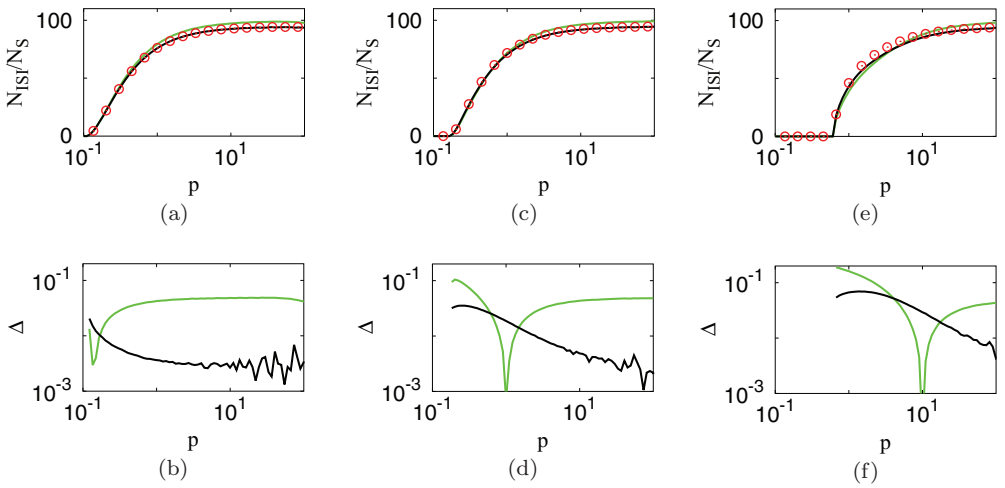

FIG. 4. (Color online) Number of ISI triples per S node as a function of infection rate, for several rewiring rates: simulations compared to two approximations. The values of the rewiring rates are as follows: $w = 10^{-1}$ in (a) and (b), $w = 10^{0}$ in (c) and (d), and $w = 10^{1}$ in (e) and (f). The curves and circles are defined as in Fig. 3, with the same values for the number of nodes and links, as well as the recovery rate.

error of the two closures,

$$\Delta = \left| 1 - \frac{\text{approximation}}{\text{exact value}} \right|, \tag{9}$$

where simulation measurements are used as the exact value.

Curiously, the homogeneity closure of N_{SSI} in Eq. (2a), together with Eq. (8), leads to the homogeneity closure in Eq. (2b). Thus, as suggested by Figs. 3 and 4, where the measured values of N_{SSI} are used, improving the closure of N_{SSI} beyond the homogeneity assumption leads to improvement of the N_{ISI} closure. In fact, Figs. 3(b), 3(d), and 3(f), as well as 4(b), 4(d), and 4(f) show the relative deviation of the closure relations from the approximated quantity and suggest that the new approximation in Eq. (8) is superior to the relation in Eq. (2b). Note that the only time the homogeneity closure appears to perform better is when it intersects the measured value of N_{ISI}/N_S, and, therefore, its superiority over the performance of the new closure is rather coincidental. Further consideration of the results in Fig. 3 shows that, as we move away from the derivation regime of slow rewiring rates, the performance of the new closure diminishes, though it is still superior to the old approximation. Predictably, as shown in Fig. 4, the performance of the new approximation improves for the larger values of infection rate and outperforms the original closure even near the epidemic threshold.

Finally, we test our new closure outside of the steady state. Figure 5(a) compares the performance of the newly derived approximation to that of the homogeneity approximation. We can see that, unlike the homogeneity closure, the new closure follows the measured values of N_{ISI}/N_S very accurately. Furthermore, as shown in Fig. 5(b), the new closure of Eq. (8) performs better as the solution approaches the steady state.

III. ADAPTIVE RECRUITMENT MODEL

The other example that we consider is a model for recruitment to a cause, introduced in Ref. [12]. A society is modeled as a network in which some of its individuals represent a particular ideology and actively recruit new members. These nodes are referred to as the recruiting nodes or R nodes. The rest of the people in the society are either susceptible to recruitment or nonsusceptible, referred to as S and N nodes, respectively. The N nodes may spontaneously change their state and become S nodes, and vice versa, at rates λ_1 and λ_2, respectively. The R nodes recruit S nodes at a recruitment rate γ per contact with an S node. A schematic representation of these transitions appears in Fig. 6(a). The R nodes can improve their recruiting capability by abandoning their connections to N nodes in favor of S nodes, as shown in Fig. 6(b). This rewiring process takes place at a rate w per contact between R and N nodes. The system is open in the sense that nodes die at rate θ per node, and new nodes enter the system at rate μ. The newborn nodes are born as N nodes and attach themselves with links to σ randomly chosen nodes.

The evolution of the ensemble average of such a system is described by the set of heterogeneous mean-field equations as

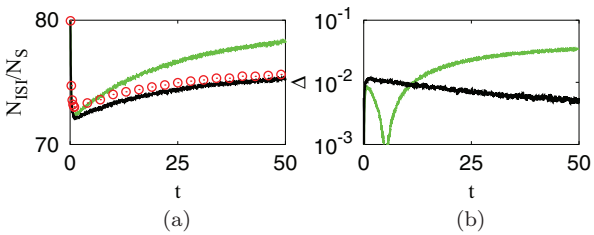

FIG. 5. (Color online) Time evolution of ISI closure. (a) The time evolution of the number of ISI triples per S node (circles, red online) and the approximate value as obtained from the relation in Eq. (2b) (light gray curve, green online) and from Eq. (8) (dark gray curve, black online). (b) The relative error due to the two approximations. The simulations are performed for $w = 10^{-1}$, $p = 10^{0}$, $r = 1$, 10^{5} nodes, and 5×10^{5} links. The initial network is a realization of an Erdös-Rényi random network; the state of each node is randomly assigned, with 90% I nodes and 10% S nodes. We take the average over 100 dynamical realizations.

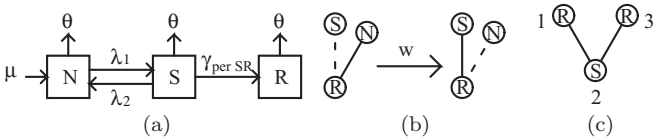

FIG. 6. (a) Schematic representation of node dynamics in the recruitment model. The nodes are born into the N class at rate μ; nodes die at rate θ; the possible transitions between the classes are marked by the arrows and labeled with the corresponding rates $(\lambda_1, \lambda_2, \gamma)$. (b) Link rewiring takes place at a rate w. Here an RN link is broken and a new RS link, based at the same R node, is created. (c) Example of a node triple.

follows:

$$\partial_t \rho_{N;\mathbf{k}} = \lambda_2 \rho_{S;\mathbf{k}} - \lambda_1 \rho_{N;\mathbf{k}} - \theta \rho_{N;\mathbf{k}} + \mu \delta_{k_1+k_2+k_3,\sigma} + \sum_i [\Omega_{N;\mathbf{k}-r_i}(r_i)\rho_{N;\mathbf{k}-r_i} - \Omega_{N;\mathbf{k}}(r_i)\rho_{N;\mathbf{k}}], \quad (10a)$$

$$\partial_t \rho_{S;\mathbf{k}} = -\lambda_2 \rho_{S;\mathbf{k}} - \gamma k_3 \rho_{S;\mathbf{k}} + \lambda_1 \rho_{N;\mathbf{k}} - \theta \rho_{S;\mathbf{k}} + \sum_i [\Omega_{S;\mathbf{k}-r_i}(r_i)\rho_{S;\mathbf{k}-\mathbf{r_i}} - \Omega_{S;\mathbf{k}}(r_i)\rho_{S;\mathbf{k}}]. \quad (10b)$$

$$\partial_t \rho_{R;\mathbf{k}} = \gamma k_3 \rho_{S;\mathbf{k}} - \theta \rho_{R;\mathbf{k}} + \sum_i [\Omega_{S;\mathbf{k}-r_i}(r_i)\rho_{S;\mathbf{k}-\mathbf{r_i}} - \Omega_{S;\mathbf{k}}(r_i)\rho_{S;\mathbf{k}}], \quad (10c)$$

where the value of $\rho_{\alpha;\mathbf{k}}$ corresponds to the expected number of α nodes with k_1 of N nodes, k_2 of S nodes, and k_3 of R nodes in their neighborhoods, with $\mathbf{k} \equiv (k_1,k_2,k_3)$. The allowed transitions and the corresponding rates are shown in Table II. In the recruiting transition rates listed in the table, function P (function Q) corresponds to the expected number of node chains that originate at a given N node (S node) with a neighborhood specified by $\mathbf{k}$ that is connected to an S node, which is turn is connected to an R node. The functions $N_{X_1 \ldots X_n}$ are defined in the same way as in Sec. II.

The mean-field equations are generated by multiplying the heterogeneous mean-field equations by $k_1^{i_1} k_2^{i_2} k_3^{i_3}$ and summing over $\mathbf{k}$, where i_1, i_2, and i_3 are non-negative integers. Thus, three node equations are generated for $i_1 + i_2 + i_3 = 0$, and six link equations are generated for $i_1 + i_2 + i_3 = 1$. These equations, presented in the Appendix as Eqs. (D1a)–(D1i), are open due to dependence on terms describing the expected number of XSR triples, N_{XSR}, with X corresponding to one of the three node states. In order to close this system of equations, additional information is required. Once again, the usual approach [15] is to assume that the R nodes are homogeneously distributed in the neighborhood of S nodes, an assumption that leads to the following closure:

$$\frac{N_{XSR}}{N_S} = \frac{N_{XS}}{N_S}\frac{N_{RS}}{N_S}, \quad (11a)$$

$$\frac{N_{RSR}}{N_S} = \left(\frac{N_{RS}}{N_S}\right)^2 + \frac{N_{RS}}{N_S}, \quad (11b)$$

where we make an additional assumption that the total degree distribution of susceptible nodes is Poisson, as was shown in Appendix B for the epidemic model.

Similarly to the previous example, these closures are *ad hoc* and are only as good as the assumptions that the closures are based on. Using the approach demonstrated in Sec. II, we derive moment closures for the triples N_{XSR} and test their accuracy against numerical simulations of the full system.

TABLE II. Transitions and nonzero transition rates in Eq. (10).

Transition	Rate
$r_1 = (-1,1,0)$	$\Omega_{N;\mathbf{k}}(r_1) = \Omega_{S;\mathbf{k}}(r_1) = \Omega_{R;\mathbf{k}}(r_1) = \lambda_1 k_1$
$r_2 = (1,-1,0)$	$\Omega_{N;\mathbf{k}}(r_2) = \Omega_{S;\mathbf{k}}(r_2) = \Omega_{R;\mathbf{k}}(r_2) = \lambda_2 k_2$
$r_3 = (-1,0,0)$	$\Omega_{N;\mathbf{k}}(r_3) = \Omega_{S;\mathbf{k}}(r_3) = \Omega_{R;\mathbf{k}}(r_3) = \theta k_1$
$r_4 = (0,-1,0)$	$\Omega_{N;\mathbf{k}}(r_4) = \Omega_{S;\mathbf{k}}(r_4) = \Omega_{R;\mathbf{k}}(r_4) = \theta k_2$
$r_5 = (0,0,-1)$	$\Omega_{N;\mathbf{k}}(r_5) = \Omega_{S;\mathbf{k}}(r_5) = \Omega_{R;\mathbf{k}}(r_5) = \theta k_3$
$r_6 = (1,0,0)$	$\Omega_{N;\mathbf{k}}(r_6) = \Omega_{S;\mathbf{k}}(r_6) = \Omega_{R;\mathbf{k}}(r_6) = \sigma\mu/(N_N + N_S + N_R)$
$r_7 = (0,-1,1)$	$\Omega_{N;\mathbf{k}}(r_7) = \gamma P(\mathbf{k})$, $\Omega_{S;\mathbf{k}}(r_7) = \gamma Q(\mathbf{k})$
$r_8 = (0,0,-1)$	$\Omega_{N;\mathbf{k}}(r_8) = wk_3$
$r_9 = (0,0,1)$	$\Omega_{S;\mathbf{k}}(r_9) = wN_{RN}/N_S$
$r_{10} = (-1,1,0)$	$\Omega_{R;\mathbf{k}}(r_{10}) = wN_{RN}/N_S$

A. Closure of NSR and SSR terms

We develop a closure of the N_{NSR} and N_{SSR} terms by considering the evolution of the expected number of node triples in the limit of $\gamma,\theta,\mu/(N_N + N_S + N_R) \ll w,\lambda_1,\lambda_2$. We consider the following expression:

$$\sum_{\mathbf{k}} \left(\frac{N_{RS}}{N_S}\frac{\partial_t \rho_{S;\mathbf{k}}}{N_N} + \frac{N_{RN}}{N_N}\frac{\partial_t \rho_{N;\mathbf{k}}}{N_N} \right)(k_1k_3 + k_2k_3). \quad (12)$$

This relation is evaluated at the steady state and using Eq. (D2a) and (D2b). After some algebraic manipulations described in Appendix E, the above relation leads to

$$\frac{N_{NSR}}{N_S} + \frac{N_{SSR}}{N_S} = \frac{N_{SN}}{N_S}\frac{N_{RS}}{N_S} + \frac{N_{SS}}{N_S}\frac{N_{RS}}{N_S}, \quad (13)$$

a result that is consistent with but does not imply the closure in Eqs. (11a) for $X = N$ and S.

We compare the asymptotically derived result of Eq. (13) and the *ad hoc* closure for the N_{SSR} term in Eq. (11a) with the corresponding values measured in the Monte Carlo simulations. Figure 7 presents the relative error [Eq. (9)] of the two closures, where simulation measurements are used as the exact value. We can see in Fig. 7(a) that the expected number of NSR and SSR triples per susceptible node, $N_{NSR}/N_S + N_{SSR}/N_S$, is well approximated (error on the order of about 1% or less) by the closure of Eq. (13) in the large λ_1 and λ_2 limit, further improving as w is increased. According to Fig. 7(c), the closure of $N_{NSR}/N_S + N_{SSR}/N_S$ continues to hold even in the parameter regime outside of the considered limit. As for the individual closures, Fig. 7(b) shows that the closure of N_{SSR}/N_S holds as well in the large λ_1 and λ_2 regime. However, as we can see in Fig. 7(d), the closure fails for small λ_1 and λ_2, especially as γ becomes dominant.

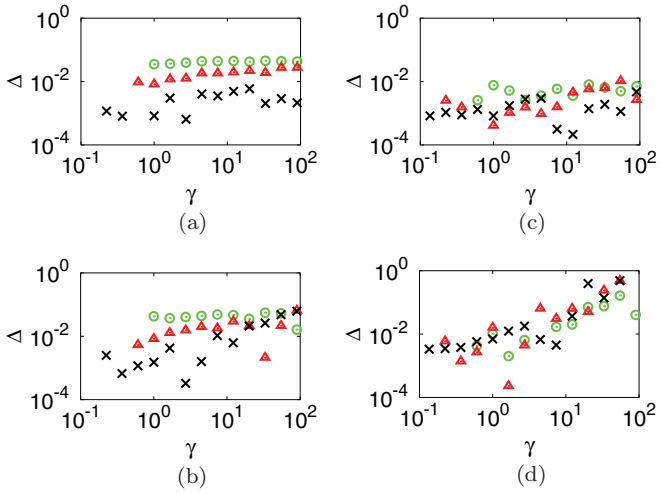

FIG. 7. (Color online) Relative errors in $N_{\mathrm{NSR}} + N_{\mathrm{SSR}}$ closure [Eq. (13)] [panels (a) and (c)] and N_{SSR} closure [Eq. (11a)] [panels (b) and (d)] at steady state, as a function of γ for $w = 10^0$ (circle, green online), $w = 10^1$ (triangle, red online), and $w = 10^2$ (cross, black online). The simulations are performed following the continuous time algorithm introduced in Ref. [25]. The values of transition rates are as follows: $\lambda_1 = 10^1$ and $\lambda_2 = 10^2$ in (a) and (b), while $\lambda_1 = 10^{-1}$ and $\lambda_2 = 10^0$ in (c) and (d). The other parameters are $\theta = 1$, $\sigma = 10$, and $\mu = 10^5$.

B. Closure of RSR term

In order to develop a closure for the N_{RSR} term, we consider the expression

$$\sum_{\mathbf{k}} k_3^2 \partial_t \rho_{S;\mathbf{k}}, \tag{14}$$

which leads to the equation describing the evolution of the expected number of RSR triples,

$$\begin{aligned}\partial_t N_{\mathrm{RSR}} = &-\lambda_2 N_{\mathrm{RSR}} - \gamma \sum_{\mathbf{k}} k_3^3 \rho_{S;\mathbf{k}}(\mathbf{k}) \\ &+ \lambda_1 N_{\mathrm{RNR}} - \theta N_{\mathrm{RSR}} + \gamma(2N_{\mathrm{RSSR}} + N_{\mathrm{SSR}}) \\ &+ w \frac{N_{\mathrm{RN}}}{N_S}(2N_{\mathrm{RS}} + N_S) + \theta(-2N_{\mathrm{RSR}} + N_{\mathrm{RS}}).\end{aligned} \tag{15}$$

Analyzing the steady state of this equation in the limit where $\gamma,\theta,\mu/(N_N + N_S + N_R) \ll w,\lambda_1,\lambda_2$, and utilizing the relations in Eqs. (D2a) and (D2b), we are able to solve this equation and obtain the following relation:

$$\frac{N_{\mathrm{RSR}}}{N_S} = \left(\frac{N_{\mathrm{RS}}}{N_S} - \frac{N_{\mathrm{RN}}}{N_N}\right)\left(2\frac{N_{\mathrm{RS}}}{N_S} + 1\right) + \frac{N_{\mathrm{RNR}}}{N_N}. \tag{16}$$

Note that, unlike the *ad hoc* closure of Eq. (11b), this result should at least be accurate in the considered limit and, therefore should be more reliable.

In order to close the N_{RNR}/N_N term in Eq. (16), we analyze the limiting behavior of the following expression:

$$\sum_{\mathbf{k}} k_3^2 [\partial_t \rho_{S;\mathbf{k}} + \partial_t \rho_{N;\mathbf{k}}], \tag{17}$$

which in steady state reduces to

$$\frac{N_{\mathrm{RNR}}}{N_N} = \frac{N_{\mathrm{RN}}}{N_N} + \frac{N_{\mathrm{RN}}}{N_N}\frac{N_{\mathrm{RS}}}{N_S}. \tag{18}$$

On substituting the result of Eq. (18) into Eq. (16), we obtain the following closure of the N_{RSR}/N_S term:

$$\frac{N_{\mathrm{RSR}}}{N_S} = 2\left(\frac{N_{\mathrm{RS}}}{N_S}\right)^2 + \frac{N_{\mathrm{RS}}}{N_S} - \frac{N_{\mathrm{RS}}}{N_S}\frac{N_{\mathrm{RN}}}{N_N}. \tag{19}$$

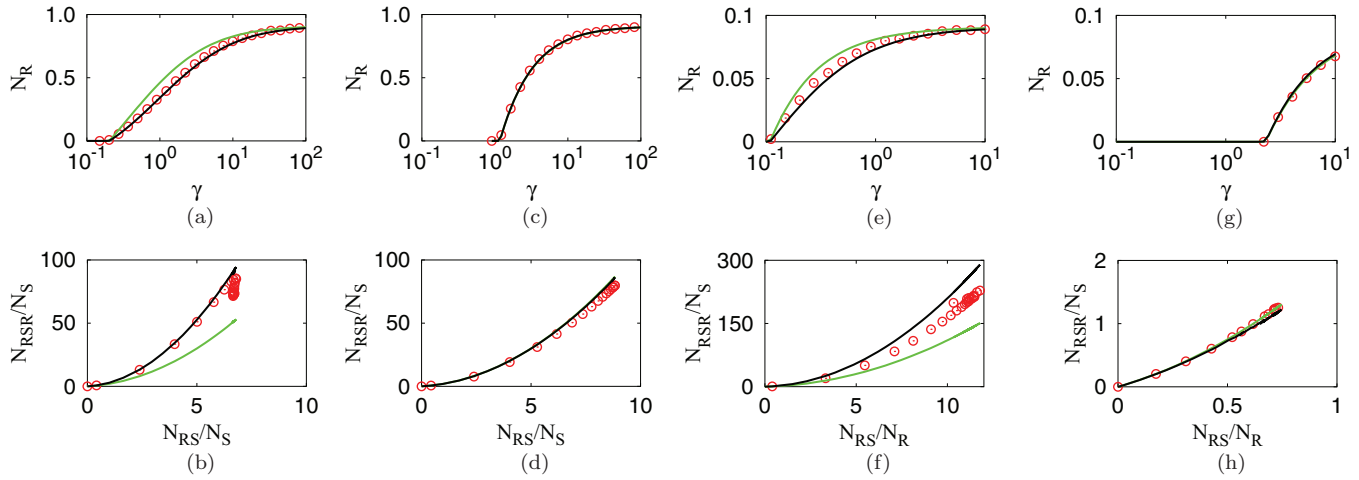

FIG. 8. (Color online) Recruitment level, N_R, and expected number of RSR triples per S node, N_{RSR}/N_S, as a function of recruitment rate γ for several sets of parameters λ_1, λ_2, and w. The values of transition rates are as follows: $\lambda_1 = 10^1$ and $\lambda_2 = 10^2$ in (a), (b), (c), and (d), while $\lambda_1 = 10^{-1}$ and $\lambda_2 = 10^0$ in (e), (f), (g), and (h). The values of rewiring rates are as follows: $w = 10^2$ in (a), (b), (e), and (f), while $w = 10^{-1}$ in (c), (d), (g), and (h). Simulation results are shown by circles (red online). In (a), (c), (e), and (g), the curves correspond to solution of mean-field equations, while in (b), (d), (f), and (h) the curves correspond to the approximation of N_{RSR}/N_S using two different closures. Dark gray curves (black online) correspond to closure in Eq. (19), while light gray curves (green online) correspond to closure in Eq. (11b). The other parameters are same as in Fig. 7. Note that in figures (c), (d), (g), and (h) the curves corresponding to the two analytic solutions lie on top of each other.

In Fig. 8, we compare the performance of the new closure of N_{RSR} in Eq. (19) to the *ad hoc*, homogeneity-based closure of Eq. (11b). We consider the numerical solution of the mean-field equations, found in Appendix D, closed according to the two methods, and compare those to the steady-state size of the recruiting class measured in the direct network simulations. In both cases, the N_{NSR} and N_{SSR} terms are closed according to the homogeneity assumption in Eq. (11a). Thus, in Fig. 8(a) we see that in the considered limit, i.e., when λ_1, λ_2, and w are large, the mean-field closed using our approach is in much better agreement with the simulations than the *ad hoc* assumption of Eq. (11b). The reason for the superior performance lies in the better approximation of the N_{RSR}/N_S term, shown in Fig. 8(b). Here N_{RSR}/N_S and N_{RS}/N_S are parametrized by γ, with larger values of N_{RS}/N_S corresponding to the larger values of γ. Notice that the performance of the closure is reduced at the larger values of γ, as the system moves outside of the considered limit.

The appeal of this approach is evident when we test it outside of the derivation limit. In Figs. 8(c) and 8(d) we see that, when we reduce w, the mean-field recruited fraction and the RSR closure continue to be in a good agreement with the simulations. We also note that in this limit the new closure approaches the homogeneity closure. We note that when the rewiring is slow relative to transitions between N and S, the expected number of R neighbors should be similar for the two node types. This would make the last term in Eq. (19) approach $(N_{\mathrm{RS}}/N_S)^2$, explaining why the two closures are close. In Fig. 8(e), as λ_1 and λ_2 are reduced, the new mean-field solution appears to be less consistent with the simulations, which is also reflected in the closure in Fig. 8(f). Finally, in Fig. 8(g), all the parameters are about the same order, and yet the asymptotically derived closure and the corresponding mean field are very much consistent with the simulations.

Thus far we have shown that our method has produced a closure that is a good match for the simulated system in steady state, and is either superior to or as good as the *ad hoc* homogeneity closure. We further test the performance of our closure by using it outside of steady state. Figures 9(a) and 9(b) show that our closure continues to be consistent with the simulations even during the transient period. This suggests that the time derivative of N_{RSR} in Eq. (15) can be neglected in the considered limit.

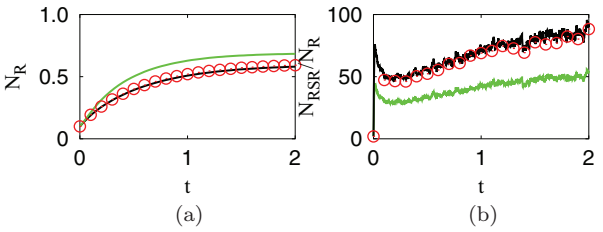

FIG. 9. (Color online) Panel (a) contains measurement and approximation of N_R. [Circles (red online)] simulation results; [light gray curve (green online)] mean field with homogeneous closure; [dark gray curve (black online)] mean field with asymptotically developed closure from Eq. (19). (b) The time evolution of the number of RSR triples per S node (circles, red online) and the approximate value obtained from the relation in Eq. (11b) (light gray curve, green online) and from Eq. (19) (dark gray curve, black online). The simulations are performed with $w = 10^2$, $\lambda_1 = 10^1$, $\lambda_2 = 10^2$, and $\gamma = 3.0$. The system evolves from a realization of Erdös-Rényi network, with mean degree 10 and 10^5 nodes, 85% of which are N nodes, 5% S nodes, and 10% R nodes. The results are averaged over 10 dynamical realizations.

IV. CONCLUSIONS AND DISCUSSION

We presented an approach for closing a mean-field description of dynamical network systems. In our approach we proposed exploiting the possible simplification of the heterogeneous mean-field description of the system in some asymptotic regime. We applied this approach to two examples of adaptive networks: a model of epidemic spread on an adaptive network and recruitment to a cause model. For the adaptive epidemic model, we took a limit of fast infection rate and slow rewiring. This led to a relationship between the triple we wished to approximate (N_{ISI}) and a four-point term (N_{ISSI}). Making a homogeneity assumption for the four-point term introduced fewer inaccuracies than making a corresponding assumption for three-point terms, presumably because correlations decay with distance between nodes. For the adaptive recruitment model, we took a limit of fast rewiring and rapid transitions between nonsusceptible and susceptible node types, relative to other transition rates. In this limit, and at steady state, equations involving nodes, links, and triples decoupled from higher-order moments, and we obtained closures for the triples in terms of nodes and links without needing to make further assumptions. However, a disadvantage is that we do not have a prescription for which asymptotic limits will do best at decoupling the hierarchy of equations, nor which will produce closures that work outside those asymptotic limits. These are areas for future study.

For both models studied here, we successfully developed closures that perform as well as or better than the usual closures, which are based on the assumptions of homogeneous distribution of nodes throughout the network. The closure we developed for the recruitment model showed significant improvement of the mean-field description over the one where all of the high-order terms were approximated using the homogeneity closure. Not only do we see an improvement in the predicted levels of the recruited population, we also see greater consistency between the moment closure approximation and direct measurements of the closed terms. Thus, of the three node-triple terms that we approximated, one showed significant improvement over the homogeneity-based closure, and the sum of the remaining two triples proved to be consistent with the homogeneity closure.

The type of results shown in Fig. 8 for the recruitment model represent what one would ideally hope to generate with this approach. We used a new closure for a triple (N_{RSR}) in the mean-field equations for nodes and links and then solved for the steady-state recruited fraction in the system. When there are n different node types, the number of node and link equations scales as n^2. In contrast, if one must consider heterogeneous mean-field equations for every possible neighborhood of a node up to a maximum degree d_{max}, the number of equations scales as d_{max}^n. The reduction in number of equations is especially drastic when nodes can have large degrees and when there are many node types.

In case of the epidemic model, the closure developed with the asymptotic approach also showed improvement over the *ad hoc*, homogeneity-based closure. The result of utilizing our approach was an improved moment closure approximation for one of the terms, contingent on improvements of a closure for the other term, as confirmed by the numerical simulations of the adaptive system. However, because another term remains to be measured in simulation or closed by some other means, we did not obtain a closed system of node and link equations as we did for the recruitment model.

It is important to note that the closures that we derived in some asymptotic regimes proved to be more accurate than the homogeneity closures even outside of the derivation limit. For example, even though in both cases the closures were derived at steady state, they showed excellent results outside of the asymptotic parameter regime where the derivation took place, as well as during the transient state of the dynamical process. The additional benefit of using this approach is that it allows us to expect good performance of the closure at least in the limit where the derivation took place, more than can be said about any *ad hoc* moment closure approximation. However, the more rigorous statements about the accuracy of this approach as well as the applicability of this approach to a more general class of network problems are left to future investigations.

ACKNOWLEDGMENTS

This work was supported by the Army Research Office, Air Force Office of Scientific Research, and Award No. R01GM090204 from the National Institute of General Medical Sciences. M.S.S. was also supported by the US National Science Foundation through Grant No. DMR-1244666. The content is solely the responsibility of the authors and does not necessarily represent the official views of the National Institute of General Medical Sciences or the National Institutes of Health.

APPENDIX A: MEAN-FIELD EQUATIONS FOR SIS WITH ADAPTATION

The mean-field equations generated from the heterogeneous mean-field equations (1a) and (1b) are as follows:

$$\partial_t N_S = rN_I - pN_{\mathrm{IS}}, \tag{A1a}$$
$$\partial_t N_I = -rN_I + pN_{\mathrm{IS}}, \tag{A1b}$$
$$\partial_t N_{\mathrm{SS}} = -2pN_{\mathrm{SSI}} + 2(r+w)N_{\mathrm{IS}}, \tag{A1c}$$
$$\partial_t N_{\mathrm{IS}} = rN_{\mathrm{II}} - pN_{\mathrm{ISI}} + pN_{\mathrm{SSI}} - (r+w)N_{\mathrm{IS}}, \tag{A1d}$$
$$\partial_t N_{\mathrm{II}} = -2rN_{\mathrm{II}} + 2pN_{\mathrm{ISI}}. \tag{A1e}$$

The conservation equations for nodes and links are

$$N_S + N_I = N, \tag{A2a}$$
$$N_{\mathrm{SS}} + 2N_{\mathrm{IS}} + N_{\mathrm{II}} = N\sigma, \tag{A2b}$$

where N is the total number of nodes and σ is the mean degree. At steady state the mean-field equations give the following relations used in the body of the paper:

$$pN_{\mathrm{SSI}} = (r+w)N_{\mathrm{IS}}, \tag{A3a}$$
$$pN_{\mathrm{ISI}} = rN_{\mathrm{II}}. \tag{A3b}$$

APPENDIX B: HOMOGENEITY CLOSURE

The homogeneity closure is based on the assumption that the probability of finding an I node at the end of a link that stems from an S node is independent of what else is in the neighborhood of that S node and is given by $q = N_{\mathrm{IS}}/(N_{\mathrm{IS}} + N_{\mathrm{SS}})$. In other words, the probability for the S node to have i of I nodes in its neighborhood is assumed to be independent of the number of S nodes in the neighborhood,

$$P_{S;n_I|n_S}(i|s) = P_{S;n_I}(i), \tag{B1}$$

where $P_{S;n_I|n_S}(i|s)$ is the probability that i of the I nodes are in the neighborhood of the S node conditioned on the presence of s of the S nodes in the neighborhood of that same S node, and $P_{S;n_I}(i)$ is the probability distribution of the number of I nodes in the neighborhood of S nodes.

When the expected number of SSI triples per S node is evaluated, the homogeneity assumption Eq. (B1) translates into the following relation:

$$\begin{aligned}\frac{N_{\mathrm{SSI}}}{N_S} &= \sum_{s,i} si\, P_{S;n_I|n_S}(i|s) P_{S;n_S}(s) \\ &= \left[\sum_i i\, P_{S;n_I}(i)\right]\left[\sum_s s\, P_{S;n_S}(s)\right] \\ &= \frac{N_{N_{\mathrm{SS}}}}{N_S}\frac{N_{\mathrm{IS}}}{N_S}.\end{aligned} \tag{B2}$$

In order to close the term describing the expected number of ISI triples per S node, additional information about the total degree distribution of S nodes, $P_{S;n_D}$, is required. We make an *ad hoc* assumption that the distribution is Poisson,

$$P_{S;n_D}(d) = \frac{e^{-\sigma}\sigma^d}{d!}, \tag{B3}$$

which would be the case had the links between the nodes been formed in a random fashion. Here the mean of the distribution is known and given by $\sigma = (N_{\mathrm{SS}} + N_{\mathrm{IS}})/N_S$. The homogeneity assumption on the distribution of I nodes implies that the probability that an S node with total degree d has i of the I nodes in its neighborhood, $P_{S;n_I|n_D}(i|d)$, is given by the binomial distribution,

$$P_{S;n_I|n_D}(i|d) = \binom{d}{i} q^i (1-q)^{d-i}. \tag{B4}$$

The expected number of ISI node triples per S node is now evaluated as follows:

$$\begin{aligned}\frac{N_{\mathrm{ISI}}}{N_S} &= \sum i^2 P_{S;n_I}(i) = \sum_{i,d} i^2 P_{S;n_I|n_D}(i|d) P_{S;n_D}(d) \\ &= \sum_d [(dq)^2 + dq(1-q)] P_{S;n_D}(d) \\ &= q^2(\sigma^2 + \sigma) + q(1-q)\sigma \\ &= q^2\sigma^2 + q\sigma = \left(\frac{N_{\mathrm{IS}}}{N_S}\right)^2 + \frac{N_{\mathrm{IS}}}{N_S}.\end{aligned} \tag{B5}$$

A similar approach leads to the homogeneity closure in the recruitment model, where we replace the infected nodes by the recruiting nodes.

APPENDIX C: DERIVATION OF THE N_{ISI} CLOSURE

Consider multiplying equation (1a) by k_2^2 and summing over $\mathbf{k}$ at steady state,

$$\sum_{\mathbf{k}} k_2^2 \partial_t \rho_{S;\mathbf{k}} = 0. \tag{C1}$$

This produces

$$\begin{aligned} 0 = {} & r N_{\mathrm{III}} - p \sum_{\mathbf{k}} \left[k_2^3 \rho_{S;\mathbf{k}}\right] \\ & + (r+w) \sum_{\mathbf{k}} \left[(k_2+1) k_2^2 \rho_{S;(k_1-1,k_2+1)} - k_2^3 \rho_{S;\mathbf{k}}\right] \\ & + p \sum_{\mathbf{k}} \left[k_2^2 K(k_1+1,k_2-1) \rho_{S;\mathbf{k}-r_2} - k_2^2 K(\mathbf{k}) \rho_{S;\mathbf{k}}\right], \end{aligned} \tag{C2}$$

which gives the result of Eq. (4) when summation indices are shifted and using the fact that $\sum_{\mathbf{k}} k_2^2 \rho_{S;\mathbf{k}} = N_{\mathrm{ISI}}$, $\sum_{\mathbf{k}} k_2 K(\mathbf{k}) \rho_{S;\mathbf{k}} = N_{\mathrm{ISSI}}$, and so on.

APPENDIX D: MEAN-FIELD EQUATIONS FOR RECRUITMENT WITH ADAPTATION

The following mean-field equations are found by multiplying Eq. (10) by $k_1^{i_1} k_2^{i_2} k_3^{i_3}$ with $i_1 + i_2 + i_3 = 0,1$:

$$\partial_t N_N = \mu - \lambda_1 N_N + \lambda_2 N_S - \theta N_N, \tag{D1a}$$

$$\partial_t N_S = \lambda_1 N_N - \lambda_2 N_S - \gamma N_{\mathrm{RS}} - \theta N_S, \tag{D1b}$$

$$\partial_t N_R = \gamma N_{\mathrm{RS}} - \theta N_R, \tag{D1c}$$

$$\begin{aligned} \partial_t N_{\mathrm{NN}} = {} & 2\sigma\mu \frac{N_N}{N_N + N_S + N_R} + 2\lambda_2 N_{\mathrm{SN}} \\ & - 2(\lambda_1 + \theta) N_{\mathrm{NN}}, \end{aligned} \tag{D1d}$$

$$\begin{aligned} \partial_t N_{\mathrm{SN}} = {} & \sigma\mu \frac{N_S}{N_N + N_S + N_R} + \lambda_2 N_{\mathrm{SS}} - \gamma N_{\mathrm{NSR}} \\ & - (\lambda_1 + \lambda_2 + 2\theta) N_{\mathrm{SN}} + \lambda_1 N_{\mathrm{NN}}, \end{aligned} \tag{D1e}$$

$$\begin{aligned} \partial_t N_{\mathrm{SS}} = {} & -2\gamma N_{\mathrm{SSR}} + 2\lambda_1 N_{\mathrm{SN}} \\ & - 2(\lambda_2 + \theta) N_{\mathrm{SS}}, \end{aligned} \tag{D1f}$$

$$\begin{aligned} \partial_t N_{\mathrm{RN}} = {} & \sigma\mu \frac{N_R}{N_N + N_S + N_R} + \gamma N_{\mathrm{NSR}} \\ & - (\lambda_1 + 2\theta + w) N_{\mathrm{RN}} + \lambda_2 N_{\mathrm{RS}}, \end{aligned} \tag{D1g}$$

$$\begin{aligned} \partial_t N_{\mathrm{RS}} = {} & -\gamma N_{\mathrm{RSR}} + \gamma N_{\mathrm{SSR}} - (\lambda_2 + 2\theta) N_{\mathrm{RS}} \\ & + (\lambda_1 + w) N_{\mathrm{RN}}, \end{aligned} \tag{D1h}$$

$$\partial_t N_{\mathrm{RR}} = 2\gamma N_{\mathrm{RSR}} - 2\theta N_{\mathrm{RR}}. \tag{D1i}$$

At steady state, in the limit where $\gamma,\theta,\mu/(N_N + N_S + N_R) \ll w,\lambda_1,\lambda_2$, Eq. (D1b) and Eq. (D1h) lead to the following relations:

$$\lambda_1 N_N = \lambda_2 N_S, \tag{D2a}$$

$$(\lambda_1 + w) N_{\mathrm{RN}} = \lambda_2 N_{\mathrm{RS}}. \tag{D2b}$$

Note that here we do not take into consideration the fact that all of the terms $N_{X_1 X_2 \ldots X_n}$ are functions of the system parameters. For example, we implicitly assume that λ_1, λ_2, and w can be chosen large enough such that $\gamma N_{\mathrm{RS}} \ll \lambda_2 N_S, \lambda_1 N_N$ in the considered limit.

APPENDIX E: DERIVATION OF THE $N_{\mathrm{NSR}} + N_{\mathrm{SSR}}$ CLOSURE.

To obtain a closure of the N_{NSR} and N_{SSR} terms in the recruiting model, we consider the expression

$$\sum_{\mathbf{k}} \left(\frac{N_{\mathrm{RS}}}{N_S} \frac{\partial_t \rho_{S;\mathbf{k}}}{N_N} + \frac{N_{\mathrm{RN}}}{N_N} \frac{\partial_t \rho_{N;\mathbf{k}}}{N_N} \right) (k_1 k_3 + k_2 k_3), \tag{E1}$$

which should be 0 at steady state. Discarding quantities proportional to parameters $\gamma,\theta,\mu/(N_N + N_S + N_R)$ (which are assumed small relative to other parameters), we find that the quantity in the first term of (E1) simplifies to

$$\begin{aligned} & \sum_{\mathbf{k}} \left(\partial_t \rho_{S;\mathbf{k}} k_1 k_3\right) \\ & = -\lambda_2 N_{\mathrm{NSR}} + \lambda_1 N_{\mathrm{NNR}} \\ & \quad + \sum_{\mathbf{k}} \Big[\lambda_1 (k_1+1) k_1 k_3 \rho_{S;\mathbf{k}-r_1} - \lambda_1 k_1^2 k_3 \rho_{S;\mathbf{k}} \\ & \quad + \lambda_2 k_1 (k_2+1) k_3 \rho_{S;\mathbf{k}-r_2} - \lambda_2 k_1 k_2 k_3 \rho_{S;\mathbf{k}} \\ & \quad + w \frac{N_{\mathrm{RN}}}{N_S} k_1 k_3 \rho_{S;\mathbf{k}-r_9} - w \frac{N_{\mathrm{RN}}}{N_S} k_1 k_3 \rho_{S;\mathbf{k}} \Big] \\ & = -\lambda_2 N_{\mathrm{NSR}} + \lambda_1 N_{\mathrm{NNR}} - \lambda_1 N_{\mathrm{NSR}} + \lambda_2 N_{\mathrm{SSR}} \\ & \quad + w \frac{N_{\mathrm{RN}}}{N_S} N_{\mathrm{SN}}, \end{aligned} \tag{E2a}$$

using the fact that $\sum_{\mathbf{k}} k_1 k_3 \rho_{S;\mathbf{k}} = N_{\mathrm{NSR}}$, $\sum_{\mathbf{k}} k_1 k_3 \rho_{N;\mathbf{k}} = N_{\mathrm{NNR}}$, and so on. Other terms in (E1) sum similarly.

We use Eqs. (D2a) and (D2b) to eliminate parameters λ_2, w from the expression (E1), replacing them with combinations of λ_1 and node and link variables. This yields

$$\begin{aligned} & \frac{1}{\lambda_1 N_N} \sum_{\mathbf{k}} [\partial_t \rho_{S;\mathbf{k}} (k_1 k_3 + k_2 k_3)] \\ & = -\frac{N_{\mathrm{NSR}}}{N_S} + \frac{N_{\mathrm{NNR}}}{N_N} + \left(\frac{N_{\mathrm{RS}}}{N_S} - \frac{N_{\mathrm{RN}}}{N_N} \right) \frac{N_{\mathrm{SN}}}{N_S} - \frac{N_{\mathrm{SSR}}}{N_S} \\ & \quad + \frac{N_{\mathrm{SNR}}}{N_N} + \left(\frac{N_{\mathrm{RS}}}{N_S} - \frac{N_{\mathrm{RN}}}{N_N} \right) \frac{2 N_{\mathrm{SS}}}{N_S} \end{aligned} \tag{E3a}$$

and

$$\begin{aligned} & \frac{1}{\lambda_1 N_N} \sum_{\mathbf{k}} [\partial_t \rho_{N;\mathbf{k}} (k_1 k_3 + k_2 k_3)] \\ & = \frac{N_{\mathrm{NSR}}}{N_S} - \frac{N_{\mathrm{RS}}}{N_S} \frac{N_N}{N_{\mathrm{RN}}} \frac{N_{\mathrm{NNR}}}{N_N} + \frac{N_{\mathrm{SSR}}}{N_S} - \frac{N_{\mathrm{RS}}}{N_S} \frac{N_N}{N_{\mathrm{RN}}} \frac{N_{\mathrm{SNR}}}{N_N} \end{aligned} \tag{E4a}$$

Combining these quantities as in (E1) and setting to 0 for steady state finally yields

$$\begin{aligned} & \left(\frac{N_{\mathrm{NSR}}}{N_S} + \frac{N_{\mathrm{SSR}}}{N_S} - \frac{N_{\mathrm{SN}}}{N_S} \frac{N_{\mathrm{RS}}}{N_S} - \frac{N_{\mathrm{SS}}}{N_S} \frac{N_{\mathrm{RS}}}{N_S} \right) \\ & \quad \times \left(\frac{N_{\mathrm{RN}}}{N_N} - \frac{N_{\mathrm{RS}}}{N_S} \right) = 0 \end{aligned} \tag{E5}$$

or

$$\frac{N_{\mathrm{NSR}}}{N_S} + \frac{N_{\mathrm{SSR}}}{N_S} = \frac{N_{\mathrm{SN}}}{N_S} \frac{N_{\mathrm{RS}}}{N_S} + \frac{N_{\mathrm{SS}}}{N_S} \frac{N_{\mathrm{RS}}}{N_S}. \tag{E6}$$

[1] R. Albert and A.-L. Barabási, Rev. Mod. Phys. **74**, 47 (2002).
[2] M. Newman, SIAM Rev. **45**, 167 (2003).
[3] S. Boccaletti, V. Latora, Y. Moreno, M. Chavez, and D. Hwang, Phys. Rep. **424**, 175 (2006).
[4] A. Arenas, A. Diaz-Guilera, J. Kurths, Y. Moreno, and C. Zhou, Phys. Rep. **469**, 93 (2008).
[5] B. Goncalves, N. Perra, and A. Vespignani, PLoS ONE **6**, e22656 (2011).
[6] K. Josic, M. Matias, R. Romo, and J. Rubin, eds., *Coherent Behavior in Neuronal Networks*, Vol. 3 of Springer Series in Computational Neuroscience (Springer-Verlag, Berlin, 2009).
[7] T. J. Sejnowski and T. Poggio, eds., *Theoretical Neuroscience: Computational and Mathematical Modeling of Neural Systems* (The MIT Press, Cambridge, MA, 2001).
[8] C. Moore and M. E. J. Newman, Phys. Rev. E **61**, 5678 (2000).
[9] R. Pastor-Satorras and A. Vespignani, Phys. Rev. E **63**, 066117 (2001).
[10] T. Gross, Carlos J. Dommar D'Lima, and B. Blasius, Phys. Rev. Lett. **96**, 208701 (2006).
[11] L. B. Shaw and I. B. Schwartz, Phys. Rev. E **77**, 066101 (2008).
[12] M. S. Shkarayev, I. B. Schwartz, and L. B. Shaw, J. Phys. A: Math. Theor. **46**, 245003 (2013).
[13] S. Jolad, W. Liu, B. Schmittmann, and R. K. P. Zia, PLoS ONE **7**, e48686 (2012).
[14] D. J. Murrell, U. Dieckmann, and R. Law, J. Theor. Biol. **229**, 421 (2004).
[15] M. J. Keeling, D. A. Rand, and A. J. Morris, Proc. R. Soc. Lond. B **264**, 1149 (1997).
[16] T. Rogers, J. Stat. Mech. (2011) P05007.
[17] M. Taylor, P. L. Simon, D. M. Green, T. House, and I. Z. Kiss, J. Math. Biol. **64**, 1021 (2012).
[18] I. Z. Kiss, L. Berthouze, T. J. Taylor, and P. L. Simon, Proc. R. Soc. A Math. **468**, 1332 (2012).
[19] I. Z. Kiss and P. L. Simon, Bull. Math. Biol. **74**, 1501 (2012).
[20] Vincent Marceau, Pierre-André Noël, Laurent Hébert-Dufresne, Antoine Allard, and Louis J. Dubé, Phys. Rev. E **82**, 036116 (2010).
[21] M. J. Keeling and K. T. D. Eames, J. R. Soc. Interface **2**, 295 (2005).
[22] A. I. Reppas, Y. De Decker, and C. I. Siettos, J. Stat. Mech. Theory Exp. (2012) P08020.
[23] T. Gross and I. G. Kevrekidis, Europhys. Lett. **82**, 38004 (2008).
[24] T. Gross and B. Blasius, J. R. Soc. Interface **5**, 259 (2008).
[25] D. Gillespie, J. Comput. Phys. **22**, 403 (1976).